Supramolecular Organization of Toluidine Blue Dye in Solid Amorphous Phases

Roberto Matassa, Claudia Sadun, Lucio D'Ilario, Andrea Martinelli, and Ruggero Caminiti*

Dipartimento di Chimica, Università degli Studi di Roma "La Sapienza" P.le A. Moro 5, I-00185 Roma, Italy

Received: October 5, 2006; In Final Form: December 20, 2006

Toluidine blue (TB) dye molecules are intensively utilized for large-area photophysics applications such as carcinoma detection, photoinactivation of bacteria, biosensors, and photovoltaic cells. Understanding the nature of the TB aggregation state becomes an essential point of the research process in order to know the structure−function relationship and to foresee technological applications of this class of metachromatic-dye molecules. However, no structural information on toluidine blue is available in the literature, maybe because of the poor crystalline character of the aggregate. Here, we present the first structural determination of TB organic molecules using the energy dispersive X-ray diffraction technique. The investigation highlights dimeric arrangements of stacked molecules in antiparallel fashion, forming a superstructure of two dimers in a transverse arrangement. The behavior of the TB higher aggregates indicates that these dye molecules, in spite of repulsion due to similar charge (cationic dyes), undergo self-aggregation to form helical conformations.

Introduction

Toluidine blue (TB) belongs to the class of thiazine dye molecules which change color when interacting with a variety of electrically charged materials. Generally, dye ions (toluidine blue, methylene blue, thionin, etc.) react with specific biological macromolecules in aqueous solution and impart to it colors which are different from those of the dye molecule. This is metachromasy, and macromolecules exhibiting such behavior are said to be metachromatic.[1,2]

The mechanism of metachromasy staining between metachromatic dyes and macromolecules in water occurs through hydrophobic interactions, involving dye−dye formation of dimers, and higher aggregates with increasing dye concentration.[3,4]

Taking advantage of the hydrophobic effects, increasing research has been focused on the utilization of TB application as an aid to the recognition and diagnosis of carcinoma in situ or invasive malignant lesions.[5−9] The valuable ability of TB molecules to permeate and accumulate in the hydrophobic region of the cellular membrane has attributed to the molecule a higher photobactericidal activity.[10−12]

The changing of spectroscopic or electrochemical properties of the TB molecules by interaction with mediators and biological molecules is arousing great interest in the field of sensors and biosensors development.[13−17]

The redox and light sensitivity properties of toluidine blue have also led to an increasing interest in photovoltaic devices because of their possible role as transducers of light to electric energy.[18−20]

Although the subject of toluidine blue dye has been considered by numerous authors, the investigations reported in the literature are mainly confined within the identification of chemical-physics properties and the aggregation occurring in solution phase.

Evidence of the degree of aggregation of the toluidine and methylene blue dissolved in water was observed by absorption spectra and confirmed by properly theoretical investigations.[21−24] The self-aggregation of metachromatic dye still occurs even when metachromatic dyes are in the form of inclusion complexes with non-metachromatic molecules, and that is aided by noncovalent interactions.[25−28]

Several optical rotation and circular dichroism studies were made to obtain information on the phenomenon of helical aggregation of metachromatic dyes in the solution phase. These investigations have shown that TB dye has a great ability to reveal the helical geometry of DNA−protein complexes as a consequence of molecular-ordered binding of TB molecules at the DNA surface.[1,29]

An interesting result was observed on helical aggregations of dye molecules bonded in a repetitive fashion to form a dye "super-helix" superimposed on a polypeptide α-helix. The asymmetric polypeptide influenced the screw sense of a dye helix located tangentially to the polypeptide α-helix. This result brought a conclusion that the helical structure of the dye cluster is an intrinsic feature of the dye−dye interaction, because the dye helix was also formed in the absence of an asymmetric chiral polymer.[30]

The energy dispersive X-ray diffraction (EDXD) technique has been chosen to study the aggregation aspect of TB samples because of the amorphous characteristics of this material. The angular dispersive X-ray diffraction (ADXD) technique also allows the study of amorphous samples by a molybdenum X-ray source, but the energy dispersive method has various advantages over the conventional angular dispersive method: the reduction of acquisition time of experimental data and the accessible region in the reciprocal space is wider.[31,32] The aim of this work is therefore to achieve more detailed information on the spatial organization and molecular interactions of toluidine blue in the solid phase, which proves to be crucial for chemical-physics properties.

Experimental Section

Sample Preparation. Toluidine Blue (TB), CA index name phenothiazin-5-ium, 3-amino-7-(dimethylamino)-2-methyl-, chloride, was purchased from Sigma Aldrich and subjected to the purification procedure reported by Pal and Shubert prior to

* To whom correspondence should be addressed. E-mail: r.caminiti@caspur.it.

10.1021/jp066555j CCC: $37.00
Published on Web 02/03/2007

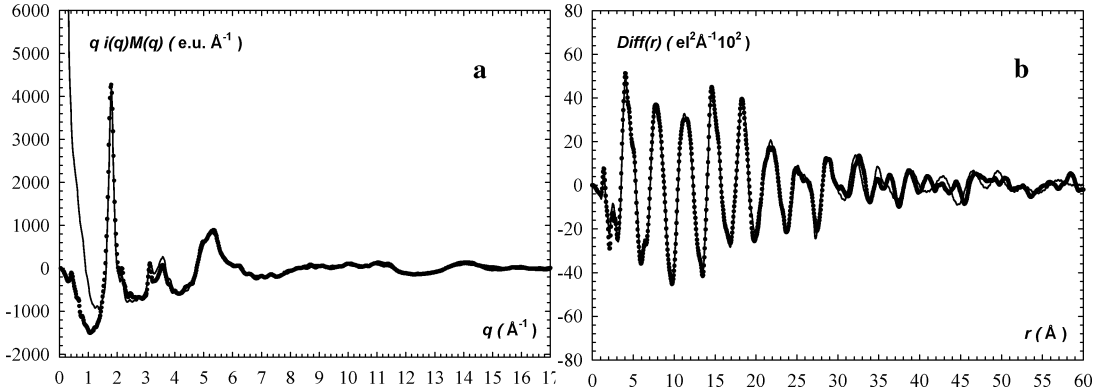

Figure 1. X-ray diffraction patterns and structural analysis of the toluidine blue dye in solid amorphous phases: (a) experimental structural function (SF) represented as dots and theoretical curve drawn as solid line calculated for 16 dimers; (b) the corresponding *Diff*(*r*) form.

use.[33] The powder samples were, then, recovered for EDXD characterization.

EDXD Data Collection and Processing. X-ray diffraction data were recorded with a custom built X-ray energy scanning diffractometer,[34,35] consisting of a Seifert X-ray HV generator supplying a water-cooled tungsten X-ray source, with a maximum power of 3.0 kW. The bremsstrahlung (braking radiation) of the X-ray source was used. The operating conditions were the following: high voltage supplies 45 kV, current intensity 35 mA. A germanium solid-state detector (SSD) was used for the diffraction spectra recording. The SSD was linked to a multichannel analyzer by an electronic chain. A set of collimating slits in front of and behind the sample, two step motors for moving arms on which the source and detector were mounted, and an adjustable sample holder placed in the optical center of the diffractometer completed the setup.

The complete experimental scattering parameter range, $q = 0.12-17.00$ Å^{-1}, was explored by performing several measurements made in correspondence with a set of scattering angles, θ, at 26.0, 15.5, 8.0, 3.5, 2.0, 1.0, and 0.5° and using the relation $q = (4\pi \sin \vartheta)/\lambda = EC \sin \vartheta$, where q is expressed in inverted angstroms and λ is expressed in angstroms; the utilized energy range is $E_{\min} = 13.5$ keV and $E_{\max} = 38.2$ keV, and the value of the constant C is 1.014 (keV·Å)$^{-1}$.

The experimental data were corrected for the following effects: escape peak suppression, normalization to the incident radiation intensity, division by X-ray absorption and polarization coefficients, and subtraction of the contributions, due to inelastic scattering, from the observed intensities $I(E, \theta)$.[36,37] Then, the spectra were joined to reconstruct the whole diffraction pattern.

Atomic scattering factors, $f_h(q)$, were taken from International Tables.[38] The experimental static structure function was calculated as

$$i(q) = I_{\text{coh}}(E,\vartheta) - \sum_h f_h^2(q) \qquad (1)$$

The experimental radial distribution, $D(r)$, was obtained as

$$D(r) = 4\pi r^2 \rho_0 + \frac{2r}{\pi}\int_0^{q_{\max}} qi(q)\, M(q) \sin(qr)\, \mathrm{d}q \qquad (2)$$

where q indicates the scattering parameter, ρ_0 is the average electronic density of the sample ($\rho_0 = (\sum_h n_h f_h^2(0))V^{-1}$), V is the stoichiometric unit volume chosen, and $M(q)$ is a modification function defined as

$$M(q) = \frac{f_S^2(0)}{f_S^2(q)} \exp(-0.01q^2)$$

TABLE 1: Final Values of the Adjusted rms σ for the Model Used

distance range (Å)	σ
$0.0 < r \le 1.8$	0.057
$1.8 < r \le 3.6$	0.103
$3.6 < r \le 8.0$	0.167
$8.0 < r \le 19.0$	0.205
$19.0 < r \le 35.0$	0.328
$35.0 < r$	0.412

The experimental structure function and the experimental radial distribution function, in the form $D_{\text{iff}}(r) = D(r) - 4\pi r^2\rho_0$, are shown in Figure 1. Theoretical peak shapes were calculated by Fourier transforming the theoretical structure function, calculated by the Debye equation for the pair interactions of the theoretical models proposed:

$$i_{mn}(q) = \sum_{m\neq n}^{N} f_m(q)\, f_n(q) \frac{\sin(r_{mn}q)}{r_{mn}q} \exp\left(-\frac{1}{2}\sigma_{mn}^2 q^2\right) \qquad (3)$$

where r_{mn} corresponds to the distance between m and n atoms and σ_{mn} is the root mean square (rms) in the interatomic distance. The number of parameters was reduced by taking the same σ value for distances falling within predefined ranges, r_{mn}, instead of using a different σ_{mn} value for each distance. The TB distance ranges of the interatomic interactions and the associated rms σ were determined, and the values are reported in Table 1.

For calculating the best agreement between experimental data and theoretical peaks, we used the following formula:

$$R_{\text{Hamilton}} = \sqrt{\frac{\sum_{i=1}^{m} ||F^{\text{e}}(q_i)| - |F^{\text{c}}(q_i)||^2}{\sum_{i=1}^{m} |F^{\text{c}}(q_i)|^2}} \qquad (4)$$

where the ith index runs over m experimental points and the e and c labels of $F(q_i)$ refer to the experimental and calculated structural functions.

Results and Discussion

The experimental structure functions (SF), $qI(q)\,M(q)$, collected in the reciprocal space in the range from 0 to 17 Å^{-1} show the typical damped oscillations of amorphous samples (Figure 1a). The SF shows a main broad peak at 1.79 Å^{-1} flanked by a less intense one at 3.14 Å^{-1} and by a second-order peak at 3.58 Å^{-1}.

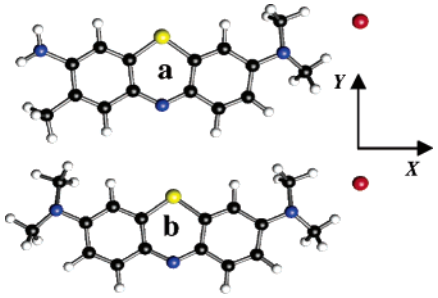

Figure 2. Chemical structures of thiazine molecules. Chloride ion, red; sulfur atom, yellow; nitrogen, blue; carbon, black; hydrogen, white: (a) toluidine blue; (b) methylene blue molecules.

This satellite peak is consistent with H type aggregation belonging to a cofacial configuration where the molecules form a vertical stack. The peak positions are closely connected to intermolecular distances, as reported by R. Caminiti et al.[39] The remaining experimental structure function shows one broad peak at 5.20 $Å^{-1}$ and two large oscillations, due to intramolecular interactions.

The Fourier transform of the structure functions yields the radial distribution function, *Diff*(*r*), from 1 to 60 Å, providing direct information about the aggregation state (Figure 1b). The first two peaks at 1.45 and 2.45 Å are attributed to the intramolecular interactions, and the peaks from 4.10 to 11.50 Å are both due to intramolecular and intermolecular interactions. All of the following peaks are assigned to the intermolecular interactions, and the less intense peaks, in the range from 32.65 to 60.00 Å, are related to the low dimension of the molecular packing.

For solving the structure, we needed to combine information gathered from the previous structural studies of thiazine dyes with that extracted by the TB models. In particular, we will report the structural studies on methylene blue (MB) molecules in the solid phase, showing similar chemical, structural, and photochemical properties as the TB molecule (Figure 2).

The first structural study on the methylene blue dye was performed by W. H. Taylor, who found a slight deformation of the molecule with the chloride ion close to the dimethylamino group.[40] The lack of planarity might probably be due to slight puckering of the molecule at the sulfur and nitrogen atoms bridging the two benzene rings.

The position of the chloride ion relative to the MB molecule has been the subject of discussion in the past. Zhdanov et al.[41] concluded that the sulfur atom of the MB cation is close to the chloride ion (2.80 Å) because of the placement of the positive charge on the sulfur atom. Marr et al. have shown that the chloride ion is close to the dimethylamino group at a distance of 4.12 Å by matching X-ray diffraction and Fourier electron-density analyses.[42,43]

Bearing in mind these premises, the starting setup for structural analysis of the toluidine blue sample was the crystal structural parameters of methylene blue.[44] A H atom replaced one methyl group at position 3, and methyl groups replaced two H atoms in position 2 for building up the model.

The apparent structural differences between methylene blue and our sample required the reoptimization of the toluidine blue geometry comparing the theoretical structural function with the experimental one in the range between 4.0 and 17.0 $Å^{-1}$. This calculation yielded a nonperfectly planar molecular configuration with the sulfur and nitrogen atoms of the heterocycle ring lying out of the molecular plane. The atomic Cartesian coordinates corresponding to this model are reported in Table 2. The chloride ion interacts with the nitrogen atom of the dimethylamino group

TABLE 2: Atomic Cartesian Coordinates (Å) of the Toluidine Blue Molecule without Hydrogen Atoms

atom	*x*	*y*	*z*	atom	*x*	*y*	*z*
Cl^-	2.46	−8.28	0.45	C	−1.51	−2.37	0.07
S	1.76	−0.00	−0.13	C	−0.72	−1.20	0.03
N	−1.34	−0.00	0.13	C	0.69	−1.37	−0.02
N	1.02	−5.09	0.03	C	0.72	1.36	−0.02
N	1.16	5.09	−0.06	C	−0.69	1.20	0.01
C	0.12	−6.07	−0.57	C	−1.45	2.41	0.01
C	2.45	−4.98	−0.31	C	−0.88	3.63	−0.01
C	1.22	−2.61	−0.05	C	0.53	3.76	−0.03
C	0.43	−3.80	−0.02	C	1.29	2.59	−0.04
C	−0.99	−3.60	0.04	C	−1.79	4.83	−0.02

at a distance of 3.52 ± 0.20 Å, showing a similar configuration to that reported by Marr et al.[42,43] The distance of the chloride ion with respect to the $N(CH_3)_2$ group is slightly different with respect to the MB.

In order to study the TB intermolecular interactions, theoretical structural analysis in comparison with the experimental one has shown that an aggregation of the H type (face to face) resolves the pair of peaks located at 1.79 and 3.58 $Å^{-1}$. To simplify the model description, the structural parameters are referred to the centers of mass of the single molecules.

Molecular stacking in a *parallel* fashion increases the intensity of the main peak, while an *antiparallel* arrangement has the opposite behavior followed by a peak appearing at 3.58 $Å^{-1}$. To recover the theoretical peak intensity at about 1.79 $Å^{-1}$, further molecules were added in the stacking configuration.

Molecular slipping also affects the main peak position. Tests were made by shifting the molecules with respect to each other along the *x*-, *y*-, or *z*-axis. A molecular slipping along the *x*- or *y*-axis causes a shifting of the main peak toward low values of *q* ($Å^{-1}$). A slipping along the *x*- and *y*-axes produces a broadening of the main peak as well as an asymmetric tail on the low *q* ($Å^{-1}$) values side followed by a decrease of intensity. The shift related to the slipping along the *z*-axis appeared to depend strongly on whether the interplanar distances were increased or reduced.

Molecular rotation around the stacking axis involves broadening and shifting effects on the main peaks. The main peak decreases considerably upon rotation around the stack axis below 20° of single molecules, while rotation of TB dimers less than 20° provides limited and favorable broadening. Dimer rotation higher than 20° yields a decrease of the main peak, shifting toward low values of *q* ($Å^{-1}$), and a spurious peak at 1.20 $Å^{-1}$ appears.

We proceeded by trying the subsequent aggregation forms, that is, dimer, trimer, tetramer, and higher aggregates.

The multistep process yields a *dimeric* aggregation state with two eclipsed molecules in the *antiparallel* configuration.

The TB dimeric structure leads to a geometry where both of the molecules are separated by 3.56 ± 0.01 Å and one of the molecules is more slipped along the *y*-axis of 0.79 ± 0.01 Å than the *x*-direction of 0.07 ± 0.01 Å with respect to the other (Figure 3a).

It is well-known that metachromatic-dye molecules have a great ability to form dimeric aggregation of the H type.[21,22] Attention must be given to the polymorphism of these organic dyes in considering their X-ray diffraction patterns. Many of them have been found to exhibit polymorphism of stacked molecules in *parallel* or *antiparallel* arrangements.

MB molecules as guest species in hydrate and pentahydrate networks have shown molecular arrangement in *parallel* fashion

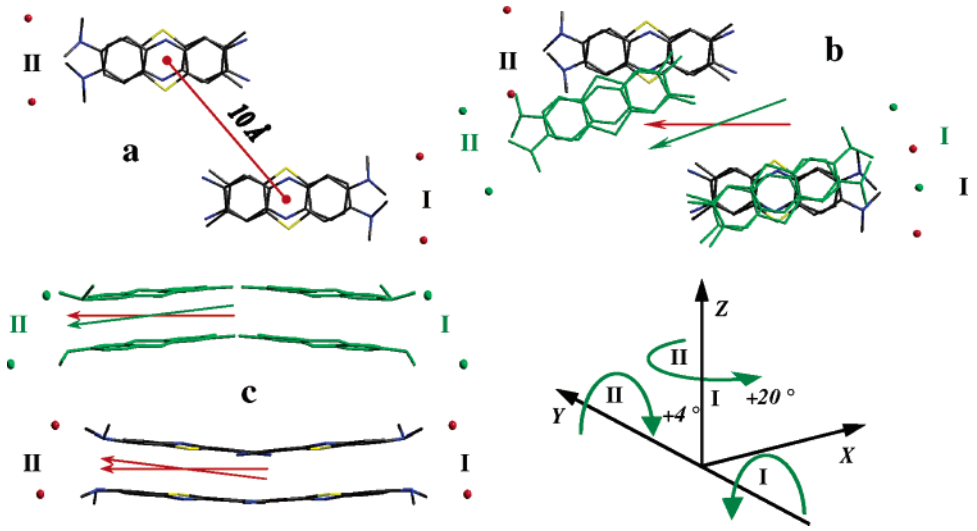

Figure 3. Structural models of the toluidine blue dimers in multistep aggregation forms: (a) *superstructure* of TB dimers in an antiparallel fashion in a *stagger* configuration; (b) top of view of two base pairs of the TB dimers in a *twist* configuration rotated around the *z*-axis of 20°; (c) two base pairs of TB dimers in a *buckle* configuration tilted in alternate mode of ±4°.

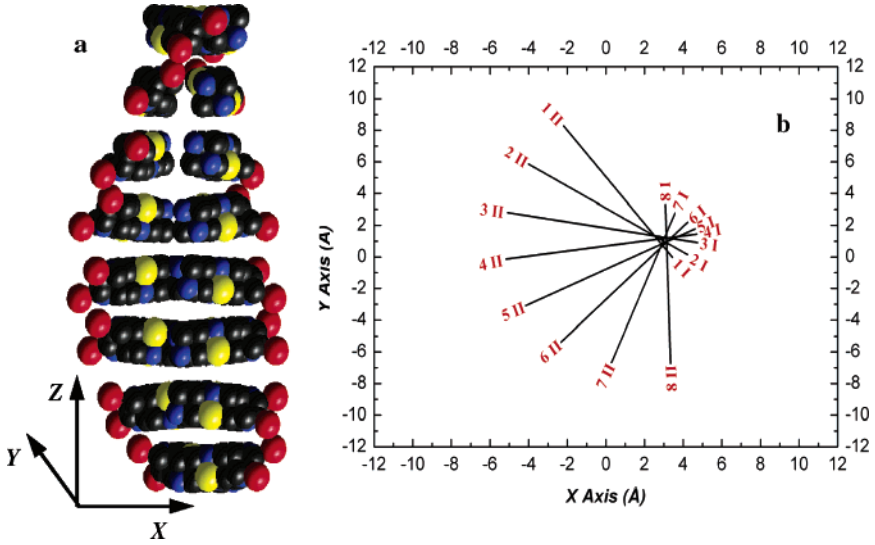

Figure 4. Supramolecular organization of toluidine blue. Proposed sketches of the TB molecular organization in a double-helix fashion: (a) 3D view; (b) Cartesian coordinate of the dimer centers of mass of the toluidine blue on the *xy*-plane. The *z*-axis is perpendicular to the graphic plane, and the label numbers increase along the *z*-axis from 1I to 8I and from 1II to 8II corresponding to two helices.

separated by an interplanar distance of ~3.47 Å and slipped along the *x*-axis with respect to the nearest molecule (Figure 2).[41,43]

In the MB−thiocyanate network, the two monomeric faces are orientated in the *antiparallel* fashion separated by 3.38 Å.[44] MB hydrate molecules incorporated in uric acid crystal have been found in recent years as dimers in the *antiparallel* configuration by an interplanar distance of 3.43 Å.[45] Structural analysis of tantalum sulfide intercalated with MB have shown the same relative positions and orientations that was found in the crystal of MB−thiocyanate.[46] MB aggregates exhibit that one of the molecules preferred to be slipped along the *y*-axis between the other stack molecules, so that the dimethylamino groups of the monomers are not in contact.

Although these values are quite similar to the *antiparallel* arrangement of TB aggregates, the slippings reported in the literature are slightly larger along the *y*-axis. This discrepancy can be explained by the presence of different peripheral groups in the TB molecule, as amine and methylene groups, which increase the interplanar distance followed by a slight molecular slipping. Moreover, several parameters influence the metachromatic-dye assembling. The molecular orientation is affected by the amount of dye content in the samples and by the presence of different conformers or molecular networks, changing the orientation of the molecules in parallel or antiparallel arrangements. In the case of the TB *antiparallel* arrangement, one has to take into account that our sample is characterized by only TBs not encapsulated within 3D molecular networks. For this reason, it is expected that the *antiparallel* fashion of metachromatic dyes might be the most stable molecular arrangement.

An accurate theoretical analysis with the experimental structural function has shown that, by adding J type dimeric arrangements, the peak at 3.14 $Å^{-1}$ and the shoulder peak at 2.16 $Å^{-1}$ appear and molecular tilting with respect to the stacking axis yields a decrease and shift of the SF toward the lower q ($Å^{-1}$) values (Figure 3a and c). Dimeric tilting in alternate mode shows broadening of the main peak without shifting, reaching a good agreement of peak area with the experimental one.

TABLE 3: Cartesian Coordinates (Å) of the TB Dimeric Centers of Mass

dimer	*x*	*y*	*z*	dimer	*x*	*y*	*z*
1I	3.44	−0.01	0.00	1II	−2.19	8.27	0.73
2I	4.22	0.15	7.10	2II	−4.01	5.86	7.83
3I	4.75	0.91	14.21	3II	−5.08	2.81	14.93
4I	4.72	1.45	21.31	4II	−5.17	−0.13	22.04
5I	4.60	1.78	28.41	5II	−4.15	−3.09	29.14
6I	4.23	2.20	35.51	6II	−2.32	−5.37	36.24
7I	3.57	2.78	42.62	7II	0.29	−6.67	43.34
8I	3.07	3.30	49.72	8II	3.34	−6.71	50.45

In this way, we are able to identify a *superstructure* of two dimers where one dimer is rotated 180° around the *z*-axis with respect to the other.

By synchronizing all structural parameters, we determined the structure of the toluidine blue sample. The experimental and theoretical SFs and *Diff*(*r*)'s are shown in parts a and b of Figure 1, respectively.

Most importantly, the best fit process brought a dimeric arrangement of eight superstructures in stacking configuration, *forming a double-helix*. A model of the TB sample is presented in Figure 4.

To describe the supramolecular organization of TB dimers, through mere noncovalent interactions, we adopt the architecture of Cambridge convention in terms of the rotational and translational parameters.[47]

The *superstructure* shows a base pair of TB dimers slipped by a *stagger* translation component, where the centers of mass of the dimers are symmetrical with respect to the origin of the *xy*-plane at a distance of 10.03 ± 0.20 Å (Figure 3a). A similar structural arrangement was found by previous results of Sours and co-workers for MB dimers placed in J type aggregation.[45]

The supramolecular organization of eight stack superstructures can be described by two rotational components: (i) the *twist* component is related to a rotation of one base pair to the next of the superstructures around the helix axis by 20 ± 2° (parallel to the *z*-axis), covering a helix circular range of 140° (Figures 3b and 4b), and (ii) the *buckle* component indicates that there is a tilting between two stack bases in alternate mode of 4 ± 1° within each single helix (Figure 3c). It is worth noticing that the stacking faults of dimers may be the prominent effect of the local structural distortion of double-helical geometry.

The amorphous behavior is characterized by an irregular slipping of the *superstructures*, represented by a system of Cartesian coordinates of the dimeric centers of mass shown in Figure 4b, and the numerical values are reported in Table 3. The centers of mass of the dimers are virtually linked by a black line having a distance of 10.00 ± 0.20 Å. The asymmetric double-helix with an average radius of 8.17 ± 0.20 Å shows that the helix axis is not located in the center of the double-helix but close to the center of mass of one dimer of the superstructure, forming an incomplete pitch of 52.79 ± 0.20 Å.

Once the supramolecular organization of TB dimers was established, a further test was made in order to check the possibility of extending the structure in the *xy*-plane. Similar columns of molecules were added in order to build up a three-dimensional structure. Several shifts and rotations of the stacks were tested, but no significant improvement of the theoretical structural function was found. The same procedure was used in ref 48.

The final fitting procedure yielded good agreement between the experimental data and theoretical peaks (Figure 1) with an R_{Hamilton} estimate error of 17.64% calculated by using eq 4.

Conclusion

The present structural studies of the solid amorphous material of toluidine blue molecules can be summarized as follows.

The structure of the single TB molecules led to the conclusion that the molecule is slightly distorted and the chloride ion is closest to the dimethylamino group of the toluidine blue cation. This result is consistent with that of the single crystal study on MB molecules,[42,43] where the crystal data of MB molecules show indisputable evidence of the atom positions and the experimental diffraction data are collected until ≈4.0 Å^{-1}. It is worth noticing that a valuable difference between the experimental data in the reciprocal space (q (Å^{-1})) suggests that by the EDXD method it is possible to expand the observable region of the q values (1.0−17.0 Å^{-1}), providing better information on the intramolecular interactions in the range between 4.0 and 17.0 Å^{-1}.

The molecular arrangement of toluidine blue exhibits a preferential configuration as the *antiparallel* fashion, forming a dimeric aggregation of the H type. This result is confirmed by a dimeric hypothesis found in the solution phase. The presence of an *antiparallel* configuration, with respect to the MB polymorphs is characterized in the sample studied and by the optimization of the dimeric interactions in an extended region of experimental data.

TB molecules are arranged into the helical aggregation, through noncovalent interactions, in agreement with circular dichroism studies in the solution phase.[30] This result brought a conclusion that the helical structures of metachromatic dyes templated by polypeptides or aminoacids are one of the more favorable interfacial packing arrangements but also an intrinsic feature of the dye−dye interactions.

The nature of the amorphous phase of the TB sample may involve the faulting effect. The dimer in an *antiparallel* fashion exhibits an anomalous stacking fault that is not observed in the crystal arrangement studies of methylene blue, which have shown constant linear molecular columns. Finally, the amorphous behavior led to local distortions of the helical geometry, resulting in an asymmetric double-helix. Consequently, the TB dimers are not able to aggregate in a complete helix, forming one-third of a complete turn around the helix axis.

Acknowledgment. The authors would like thank the INFM institute and MIUR 2004 (Ateneo Ruggero Caminiti) for financial support of this research.

References and Notes

(1) Prento, P. *Biotech. Histochem.* **1999**, *76*, 137−161.

(2) Bergeron, J. A.; Singer, M. *J. Biophys. Biochem. Cytol.* **1958**, *4*, 433−457.

(3) Antonov, L.; Gergov, G.; Petrov, V.; Kubista, M.; Nygren, J. *Talanta* **1999**, *49*, 99−106.

(4) Rabinowitch, E.; Epstein, L. F. *J. Am. Chem. Soc.* **1941**, *63*, 69−78.

(5) Gandolfo, S.; Pentenero, M.; Broccoletti, R.; Pagano, M.; Carrozzo, M.; Scully, C. *Oral Oncol.* **2006**, *42*, 89−95.

(6) Li, R.; Yaun, R.; Chai, Y.; Zhang, L.; Zhuo, Y.; Zhang, Y. *J. Biotechnol.* **2006**, *123*, 356−366.

(7) Zhang, L.; Williams, M.; Poh, C. F.; Laronde, C. F.; Epstein, J. B.; Durham, S.; Nakamura, H.; Berean, K.; Hovan, A.; Le, N. D.; Hislop, G.; Priddy, R.; Hay, J.; Lam, W. L.; Rosin, M. P. *Cancer Res.* **2005**, *65*, 8017−8021.

(8) Egozcue, J.; Mirò, R.; Gelabert, A.; Algaba, F. *Cancer Genet. Cytogenet.* **2004**, *155*, 89−91.

(9) Onofre, A. M.; Sposto, M. R.; Navarro, C. M. *Oral Surg., Oral Med., Oral Pathol.* **2001**, *91*, 535−540.

(10) Wainwright, M. *Dyes Pigm.* **2007**, *73*, 7−12.

(11) Williams, J. A.; Pearson, G. J.; Colles, M. J.; Wilson, M. *Caries Res.* **2004**, *38*, 530−536.

(12) Usacheva, M. N.; Teichert, M. C.; Biel, M. A. *J. Photochem. Photobiol., B* **2003**, *71*, 87−98.
(13) Chen, S.; Yuan, R.; Chai, Y.; Xu, L.; Wang, N.; Li, X.; Zhang, L. *Electroanalysis* **2006**, *18*, 471−477.
(14) Jiao, K.; Li, Q. J.; Sun, W.; Wang, Z. J. *Electroanalysis* **2005**, *11*, 997−1002.
(15) Tian, F.; Zhu, G. *Sens. Actuators, B* **2004**, *97*, 103−108.
(16) Ribeiro, E. S.; Dias, S. L. P.; Fujiwara, S. T.; Gushichem, Y.; Bruns, R. E. *J. Appl. Electrochem.* **2003**, *33*, 1069−1075.
(17) Ju, H.; Xiao, Y.; Lu, X.; Chen, H. *J. Electroanal. Chem.* **2002**, *518*, 123−130.
(18) Jana, A. K. *J. Photochem. Photobiol., A* **2000**, *132*, 1−17.
(19) Gangotri, K. M.; Meena, R. C.; Meena, R. *J. Photochem. Photobiol., A* **1999**, *123*, 93−97.
(20) Ilanchelian, M.; Retna, Raj, C.; Ramaraj, R. *J. Inclusion Phenom.* **2000**, *36*, 9−20.
(21) D'Ilario, L.; Martinelli, A. *Modell. Simul. Mater. Sci. Eng.* **2006**, *13*, 1−15.
(22) Mukerjee, P.; Ghosh, A. K. *J. Am. Chem. Soc.* **1970**, *92*, 6419−6424.
(23) Braswell, E. *J. Phys. Chem.* **1968**, *72*, 2477−2483.
(24) Schubert, M.; Levine, A. *J. Am. Chem. Soc.* **1955**, *77*, 4197−4201.
(25) Yurehli, K.; Conley, E.; Krishnamoorti, R. *Langmuir* **2005**, *21*, 5825−5830.
(26) Patil, K.; Pawara, R.; Talap, P. *Phys. Chem. Chem. Phys.* **2000**, *2*, 4313−4317.
(27) Bergmann, K.; O'Konski, C. T. *J. Phys. Chem.* **1963**, *67*, 2169−2177.
(28) Levine, A.; Schubert, M. *J. Am. Chem. Soc.* **1952**, *74*, 91−97.
(29) De Campos Vidal, B. *Cell Biol. Int.* **2000**, *24*, 723−728.
(30) Stryer, L.; Blout, E. R. *J. Am. Chem. Soc.* **1961**, *83*, 1411−1418.
(31) Egami, T. *J. Appl. Phys.* **1979**, *50*, 1564−1569.
(32) Murata, Y.; Nishikawa, K. *Bull. Chem. Soc. Jpn.* **1978**, *51*, 411−418.
(33) Pal, M. K.; Schubert, M. *J. Am. Chem. Soc.* **1962**, *84*, 4384−4393.
(34) Caminiti, R.; Sadun, C.; Rossi Alberini, V.; Cilloco, F.; Felici, R. XXV Italian Congress on Physical Chemistry, Cagliari, Italy, 1991.
(35) Caminiti, R.; Sadun, C.; Rossi Alberini, V.; Cilloco, F.; Felici, R. Patent no. RM/93 01261484, June 23, 1993.
(36) Nishikawa, K.; Iijima, T. *Bull. Chem. Soc. Jpn.* **1984**, *57*, 1750−1759.
(37) Fritsch, G.; Keimel, D. A. *Mater. Sci. Eng., A* **1991**, *134*, 888−892.
(38) *International Tables for X-ray Crystallography*; Kynoch Press: Birmingham, England, 1974; Vol. 4.
(39) Caminiti, R.; Capobianchi, A.; Marovino, P.; Paoletti, A. M.; Padeletti, G.; Pennesi, G.; Rossi, G. *Thin Solid Films* **2001**, *382*, 70−80.
(40) Taylor, W. H. *Z. Krystallogr.* **1935**, *91*, 450−460.
(41) Zhdanov, G. S.; Zvonkova, Z. V.; Vorontsova, L. G. *Sov. Phys. Crystallogr.* **1956**, *1*, 44−48.
(42) Marr, H. E., III: Stewart, J. M. *Chem. Commun.* **1971**, 131.
(43) Marr, H. E., III; Stewart, J. M.; Chiu, M. F. *Acta Crystallogr., Sect. B* **1973**, *29*, 847−853.
(44) Kahn-Harari, A.; Ballare, R. E.; Norris, E. K. *Acta Crystallogr., Sect. B* **1973**, *29*, 1124−1126.
(45) Sours, R. E.; Fink, D. A.; Swift, J. A. *J. Am. Chem. Soc.* **2002**, *124*, 8630−8636.
(46) Capkovà, P.; Pospìsil, M.; Lerf, A. *Solid State Sci.* **2002**, *4*, 671−676.
(47) Dickerson, R. E.; Bansal, M.; Calladine, C. R.; Diekmann, S.; Hunter, W. N.; Kennard, O.; von Kitzing, E.; Lavery, R.; Nelson, H. C. M.; Olson, W. K. *J. Mol. Biol.* **1989**, *205*, 787−791.
(48) Matassa, R.; Cervone, E.; Sadun, C. *J. Porphyrins Phtalocyanines* **2003**, *7*, 579−584.